Synthesis of Carbide-Derived Carbon by Chlorination of Ti_2AlC

Elizabeth N. Hoffman, Gleb Yushin, Michel W. Barsoum, and Yury Gogotsi*

Department of Materials Science and Engineering and A. J. Drexel Nanotechnology Institute, Drexel University, Philadelphia, Pennsylvania 19104

Received December 23, 2004. Revised Manuscript Received February 22, 2005

Nanoporous carbide-derived carbon (CDC) was synthesized starting with Ti_2AlC powders via chlorination in the 400−1200 °C temperature range. X-ray diffraction, Raman spectroscopy, and transmission electron microscopy (TEM) confirmed a structural dependence on chlorination temperature. At low chlorination temperatures, the CDC structure appeared primarily amorphous. Graphitic ribbons, as well as sharply bent graphitic structures, were observed at 800 °C. As the chlorination temperature was further increased to 1000 °C, the width of the graphitic ribbon increased. No significant increase in graphitization occurred between 1000 and 1200 °C. Sorption measurements determined the presence of micropores (0.40−2.0 nm) after chlorination at 400 °C; chlorination at 800 °C or higher resulted in both micro- and mesopores (0.35 to >7 nm).

Introduction

Nanoporous carbon, due to its high specific surface area and nanosized pores, can be used for filtration, gas separation, gas storage, and electrochemical applications.[1−10] Carbide-derived carbons (CDCs) have a tunable, narrow pore size distribution as compared to other highly porous carbon materials.[1] The pore size distribution depends on the initial carbide, both structure and composition, and the CDC processing parameters. CDCs can be produced through a chlorination process, by which non-carbon elements are selectively etched from the carbide via reaction with chlorine, Cl_2, at elevated temperatures. During the process, the resulting CDC retains the shape of the original carbide. Various binary carbides have been used for CDC synthesis.[4,6−8] More recently, it has been shown that chlorination of ternary carbides, such as Ti_3SiC_2, results in CDCs with larger pore volumes and more precise control over the pore size.[11,12] As important, it was demonstrated that the pore size was a function of chlorination temperature.

Ti_3SiC_2 and Ti_2AlC are ternary carbides belonging to the $M_{n+1}AX_n$ family where n is an integer 1, 2, or 3, M is an early transition element, A is an A-group element, and X is either carbon and/or nitrogen. MAX-phase carbides are readily machinable because of their lamellar structure.[13] CDCs produced from Ti_2AlC should have a lower theoretical carbon density [0.37 g/cm^3], and a lower a/c ratio as compared to Ti_3SiC_2's unit cell.[13] Therefore, it is reasonable to expect a different pore size distribution in CDCs produced from Ti_2AlC.

This paper describes the formation and structural evolution of CDCs produced from Ti_2AlC in the 400−1200 °C temperature range and compares the results to CDCs produced from Ti_3SiC_2 and other carbides.

Materials and Experimental Section

Chlorination was preformed on commercially available polycrystalline Ti_2AlC powder (3ONE2, LLC, NJ). Reactive and purging gases used during chlorination experiments were high purity Cl_2 (BOC Gases, 99.5%) and high purity Ar (BOC Gases, 99.998%), respectively.

Details of the chlorination apparatus and synthesis procedure can be found elsewhere.[1] In brief, the Ti_2AlC powder was loaded into a horizontal quartz tube furnace. The tube was purged with Ar for 30 min, followed by heating to the desired temperature at the rate of 30 °C/min. A bubbler containing sulfuric acid was attached to the exhaust tubing to prevent back-flow of air into the system. Once the desired temperature was achieved, the Ar flow was stopped and the Cl_2 flow was started at a rate of 10 sccm. After 3 h at temperature, the sample was cooled under an Ar environment to remove residual metal chlorides.

FactSage v. 5.2 Gibbs free energy minimization program (GTT Technologies, Germany) was used to estimate the equilibrium

* To whom correspondence should be addressed. E-mail: gogotsi@drexel.edu.

(1) Nikitin, A.; Gogotsi, Y. Nanostructured Carbide-Derived Carbon. In *Encyclopedia of Nanoscience and Nanotechnology*; Nalwa, H. S., Ed.; American Scientific Publishers: 2003; Vol. 7, p 553.
(2) Barata-Rodrigues, P. M.; Mays, T. J.; Moggridge, G. D. *Carbon* **2003**, *41*, 2231.
(3) Lee, S. M.; Kaneko, K. *Carbon* **2003**, *41*, 374.
(4) Gordeev, S. K. Nanoporous and Nanofragmental Carbon Composite Materials. In *NATO ASI on Nanostructured Carbon for Advanced Applications*; Benedek, G., Milani, P., Ralchenko, V. G., Eds.; Kluwer Academic Publishers: Dordrecht, 2001; p 71.
(5) Ersoy, D. A.; McNallan, M. J.; Gogotsi, Y. *J. Electrochem. Soc.* **2001**, *148*, C774.
(6) Kotina, I. M.; Lebedev, V. M.; Ilves, A. G.; Patsekina, G. V.; Tuhkonen, L. M.; Gordeev, S. K.; Yagovkina, M. A.; Ekström, T. *J. Non-Cryst. Solids* **2002**, *299*−*302*, 815.
(7) Kotina, I. M.; Lebedev, V. M.; Ilves, A. G.; Patsekina, G. V.; Tuhkonen, L. M.; Gordeev, S. K.; Yagovkina, M. A.; Ekström, T. *J. Non-Cryst. Solids* **2002**, *299*−*302*, 820.
(8) Dash, R. K.; Nikitin, A.; Gogotsi, Y. *Microporous Mesoporous Mater.* **2004**, *72*, 203.
(9) Nijkamp, M. G.; Raaymakers, J. E. M. J.; van Dillen, A. J.; de Jong, K. P. *Appl. Phys. A* **2001**, *72*, 619.
(10) Strano, M. S.; Foley, H. C. *Carbon* **2002**, *40*, 1029.
(11) Gogotsi, Y.; Nikitin, A.; Ye, H.; Zhou, W.; Fischer, J. E.; Yi, B.; Foley, H. C.; Barsoum, M. W. *Nat. Mater.* **2003**, *2*, 591.
(12) Yushin, G.; Hoffman, E. N.; Nikitin, A.; Ye, H.; Barsoum, M. W.; Gogotsi, Y. *Carbon* **2005**, in press.
(13) Barsoum, M. W. *Prog. Solid State Chem.* **2000**, *28*, 201.

10.1021/cm047739i CCC: $30.25
Published on Web 03/29/2005

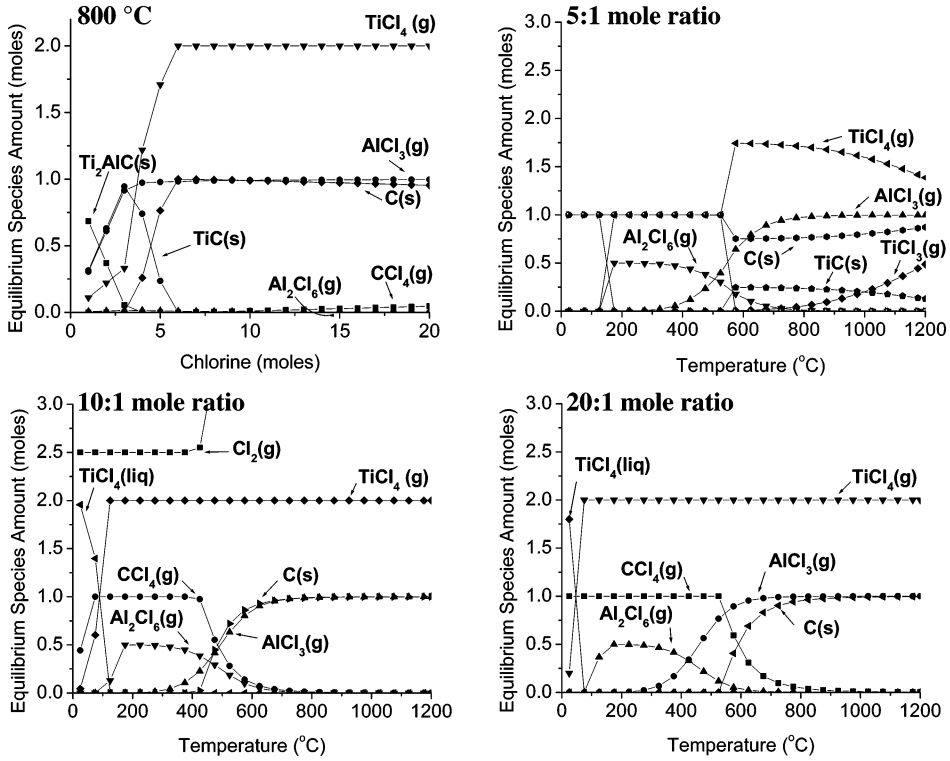

Figure 1. Thermodynamic simulations of Ti_2AlC chlorination at 1 atm with constant: (a) temperature of 800 °C, (b) Cl_2:Ti_2AlC mole ratio of 5:1, (c) 10:1, (d) 20:1.

amounts of reaction species as a function of the amount of Cl_2 and chlorination temperature. The thermodynamic calculations were performed assuming a closed system with a constant total pressure of 1 atm. The gas phase was considered to be a mixture of ideal gases, and the solid phase was treated as a mechanical mixture of compounds with unit activities.

X-ray diffraction (XRD) analysis was done on a Geigerflex diffractometer (Rigaku, Japan) using Cu Kα radiation with an accelerating voltage of 35 kV, current of 40 mA, 2θ-step of 0.05, and a hold time of 2 s. Micro-Raman spectroscopy was performed using an Ar ion laser excitation (514.5 nm) on a Ramascope 1000 Raman microspectrometer (Renishaw, UK) equipped with a charged coupled device (CCD) detector and an optical microscope for focusing the incident laser beam to a 1−2 μm spot size. Multiple Raman spectra were collected for each chlorination temperature; the average spectrum was calculated and used for analysis. High-resolution transmission electron microscopy (HRTEM) was used to observe the CDC structure. The TEM samples were prepared by a 15 min sonication of the CDC powder in 2-propanol and deposition on the lacy-carbon coated copper grid (200 mesh). A field-emission TEM (JEOL 2010F) with an imaging filter (Gatan GIF) was used at 200 kV.

Argon absorption of the powder samples was carried out using a Quantachrome Autosorb-1. Prior to the analysis, the powders were outgassed in a helium environment for 1/2 h at 60 °C followed by 10 h at 300 °C. The sorption isotherm (quantity of Ar adsorbed onto, or desorbed, from the CDC surface at various pressures) was measured at −196 °C and analyzed using the BET (Brunauer, Emmet, and Teller) and DFT (Density Functional Theory) methods to determine the specific surface area (SSA) and pore size distribution. While in microporous materials with assumed slit pore shape, DFT calculations are believed to be most accurate, BET calculations, having been used historically, are included for the purpose of comparison with previously published data.

Results and Discussion

Reaction Thermodynamics. To help predict optimum synthesis parameters, thermodynamic simulations can be used.[14] The thermodynamic calculations for the chlorination of Ti_2AlC, considering a closed system, are shown in Figure 1. The equilibrium amount of each reaction species varies with chlorination temperature and amount of initial Cl_2. The Ti_2AlC chlorination in the presence of low amounts of Cl_2 does not allow the completion of the CDC transformation, thus producing less carbon as compared to higher Cl_2 amounts. Figure 1a shows the expected equilibrium amount of carbon at 800 °C will plateau at a maximum carbon yield at 6 mol of Cl_2 or higher. At higher amounts of Cl_2, the carbon yield falls slightly due to the formation of gaseous CCl_4. Insufficient amount of Cl_2 may also result in the formation of solid $TiCl_3$ at temperatures below ∼600 °C (Figure 1b). As the mole ratio of Cl_2 to Ti_2AlC is increased, carbon becomes the only solid stable over the entire temperature range. Interestingly, higher Cl_2 amounts result in an increase in the temperature where the maximum carbon yield starts to plateau. Increasing the Cl_2 content from a mole ratio of 10:1 to 20:1 results in the increase in this temperature from ∼650 °C (Figure 1c) to ∼800 °C (Figure 1d). The thermodynamic simulations convey an optimum Cl_2:Ti_2AlC ratio where maximum carbon is produced over a large temperature range: adding too much or too little Cl_2 will decrease the temperature range, yielding maximum carbon. Note a decrease in carbon yield is possible at high Cl_2 amounts due to the extended formation of CCl_4.

(14) Jacobson, N. S.; Gogotsi, Y. G.; Yoshimura, M. *J. Mater. Chem.* **1995**, *5*, 595.

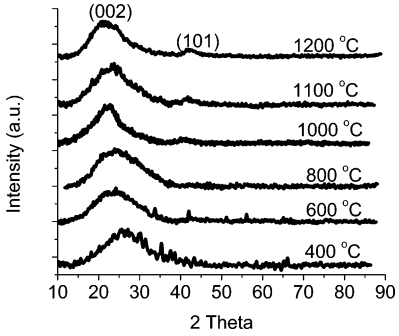

Figure 2. Powder X-ray diffraction patterns after chlorination at temperatures indicated.

High carbon yields produced from Ti_2AlC are expected at elevated chlorination temperatures and intermediate to high amounts of Cl_2, similar to Ti_3SiC_2-based carbon.[12] The chlorination temperature at which the maximum carbon yield occurs increases with the amount of Cl_2 for Ti_2AlC; similar results have been documented for Fe_3C, SiC, TiC, and Ti_3SiC_2.[1,12,15]

Powder X-ray Diffraction. X-ray diffraction confirmed the transformation from crystalline Ti_2AlC to carbon at temperatures of 400 °C and above. The peak at ~26°, due to diffraction from the (002) planes of graphite, is weak and broad due to a very small crystallite size, in the whole temperature range under study (Figure 2). The average crystallite size was calculated, using the Scherrer equation, to increase from ~0.85 to ~1.0 nm as the chlorination temperature increased from 600 to 1200 °C. A similar trend was found in carbon produced from Ti_3SiC_2.[12] As the chlorination temperature increased to ~1000 °C and above, a peak at ~44° formed (Figure 2). This peak is due to diffraction from the (101) planes of graphite and presumably corresponds to growth and widening of the graphite ribbons.

Raman Spectroscopy Analysis. The carbon ordering within the CDC was determined using Raman spectroscopy. Perfect graphite clearly shows only one Raman active mode, the G-band, located at 1582 cm^{-1}. This peak corresponds to graphite in-plane vibrations with E_{2g} symmetry.[16,17] Defective graphite and disordered carbons generally show at least two additional bands; one at ~1350 cm^{-1} (D-band) and one at ~1620 cm^{-1} (D′-band) for an excitation at wavelength $\lambda =$ 488 nm.[18,19] The position of these bands may vary considerably, depending on the structure of the disordered carbon and the excitation wavelength.[20−22] The D-peak is generally associated with breathing vibrations of sp^2 rings, which the A_{1g} symmetry disallows in graphite,[21,23] or with a double-resonance Raman process in disordered carbon.[24] In the case of a double-resonance effect, any phonon mode irrespective of the symmetry can give rise to the D-peak if the wave vector of the phonon is twice as large as the wave vector of the electronic transition excited by the incident phonon. The D′-peak is believed to correspond to a strong maximum in the vibrational density of states (VDOS) of graphite.[18] It is well known that in amorphous materials with no close order, the breakdown of the selection rules leads to Raman spectra that reflect the VDOS in their crystalline counterparts.[25]

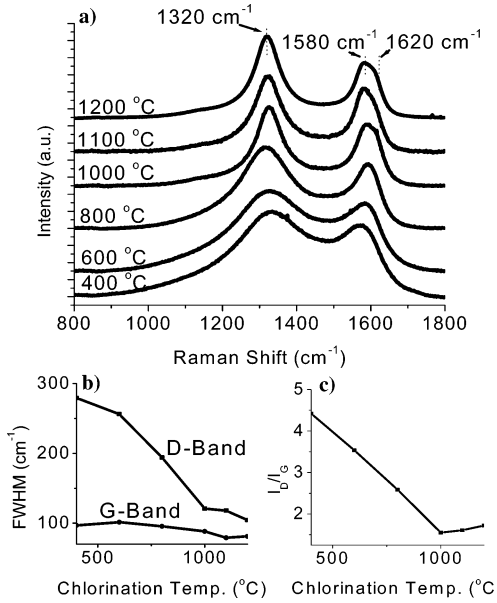

Figure 3. Raman analysis of CDC: (a) spectra of powders at varying chlorination temperatures, (b) fwhm of the D-band and G-band peaks versus chlorination temperature, and (c) I_G/I_D versus chlorination temperature.

Raman microanalysis of samples prepared in the 400−1200 °C temperature range exhibited strong peaks for both D- and G-bands, confirming the conversion to carbon (Figure 3). For simplicity, we used a two-band approximation, where only D- and G-bands (Figure 3a) were taken into account for the analysis of the spectra. No significant peak shift was observed for either band as a function of synthesis temperature. The change in full width at half-maximum (fwhm) of the G-band was minimal (Figure 3b), but a separation of the G-peak into two separate maxima at 1582 cm^{-1} (actual G-band) and ~1610 cm^{-1} (D′-band) at above 1000 °C indicated an increase in graphitic carbon at higher temperatures. As the chlorination temperature increases from 400 to 1000 °C, the D-band narrows significantly; after chlorination at 1000−1200 °C, the narrowing rate is diminished. The ratio of integrated intensities of the D-band and G-band (I_D/I_G) decreased with increasing temperature up to 1000 °C (Figure 3c), reaching a minimum at 1000 °C, after which it increased marginally with increasing temperature to 1200 °C. Both of these observations suggest that most of the ordering occurs between 400 and 1000 °C. This ordering is manifested in an increase in the size of graphite crystallites (Figure 3b), together with a decrease in the number of unsaturated sp^2 carbon bonds (Figure 3c).

(15) Dimovski, S. N. A.; Ye, H.; Gogotsi, Y. *J. Mater. Chem.* **2004**, *14*, 238.
(16) Nemanich, R. J.; Lukovsky, G.; Solin, S. A. In *Proc. Int. Conf. on Lattice Dynamics*; Balkanski, M., Ed.; Flammarion Press: Paris, 1975; p 619.
(17) Tuinstra, F.; Koenig, J. L. *J. Chem. Phys.* **1970**, *53*, 1126.
(18) Nemanich, R. J.; Solin, S. A. *Phys. Rev. B* **1979**, *20*, 392.
(19) Vidano, R. P.; Fishbach, D. B.; Willis, L. J.; Loehr, T. M. *Solid State Commun.* **1981**, *39*, 341.
(20) Ferrari, A. C. *Diamond Relat. Mater.* **2002**, *11*, 1053.
(21) Ferrari, A. C.; Robertson, J. *Philos. Trans. R. Soc. London* **2004**, *362*, 2477.
(22) Negri, F.; di Donato, E.; Tommasini, M.; Castiglioni, C.; Zerbi, G.; Mullen, K. *J. Chem. Phys.* **2004**, *120*, 11889.
(23) Mapelli, C.; Castiglioni, C.; Meroni, E.; Zerbi, G. *J. Mol. Struct.* **1999**, *481*, 615.
(24) Thomsen, C.; Reich, S. *Phys. Rev. Lett.* **2000**, *85*, 5214.
(25) Shuker, R.; Gammon, R. W. *Phys. Rev. Lett.* **1970**, *25*, 222.

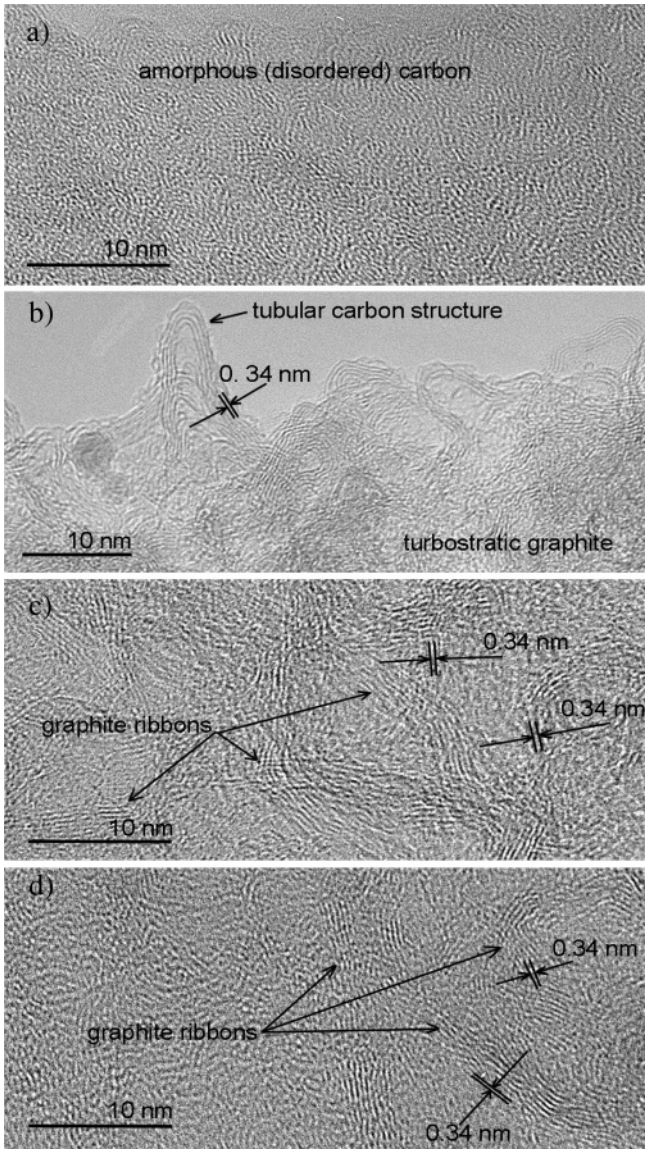

Figure 4. HRTEM micrographs of CDC chlorinated at (a) 400 °C, (b) 800 °C, (c) 1000 °C, and (d) 1200 °C.

Transmission Electron Microscopy. HRTEM images of powder samples revealed that samples chlorinated at 400 °C were comprised mainly of amorphous carbon (Figure 4a). Increasing the processing temperature to 800 °C resulted in the formation of various graphitic structures, which were often sharply twisted at the edges of most particles with characteristics similar to those of multiwalled nanotubes (Figure 4b). Similar curved graphitic structures were also observed in CDC produced at 800 °C from Ti_3SiC_2.[12] A considerable amount of amorphous and turbostratic carbon was also present in this sample. A significant jump in the degree of graphitization was observed in samples chlorinated above 1000 °C (Figure 4c,d). These CDCs consisted of graphite ribbon networks and amorphous carbon. No curved graphitic structures were found in these samples. Surprisingly, CDCs produced at 1000 and 1200 °C exhibited similar morphologies. No significant changes in ribbon thickness were noticed. In general, the TEM results agree well with the XRD and Raman spectroscopy results. All characterization tools suggest ordering of the CDC at elevated temperatures and small differences in the CDCs prepared in the 1000−1200 °C temperature range.

It is interesting to note that, according to Boehm,[26] carbon nanotubes (CNT) were first observed in 1972, during TEM analysis of CDC produced from SiC. Boehm observed multiwall CNTs and C onions only occasionally in CDCs and concluded that these structures were present in the SiC before the chlorination. However, we believe that nanotube synthesis during the CDC production is possible. Gogotsi et al. reported the formation of carbon onions and CNT in CDC from SiC.[1,27] Welz observed CNT and carbon onions in CDC produced from SiC and TiC.[28] Kusunoki et al. discovered growth of self-organized CNT films by thermal decomposition of SiC in a vacuum.[29] Zheng et al.[30] found carbon onions in CDC produced from TiC. Similar multiwall nanostructures were also observed in large quantities in CDCs produced from Al_4C_3.[31−33] Mechanisms governing the growth of various nanostructures during chlorination of carbides are not yet clear. A catalytic effect of impurities present in carbides,[32] metals, or metal chlorides might play a significant role in the nanostructure formation. Carbide structure and optimum temperature regime also seem to be important parameters for the selective synthesis of various nanostructures. Further investigation is needed to clarify the observed phenomena.

Specific Surface Area and Pore Size Distribution. The Ar adsorption isotherms of samples chlorinated in the 400−1200 °C temperature range are shown in Figure 5a. The 400 and 600 °C samples' isotherms are of type I of the Brunauer classification.[34] This isotherm type is consistent with a microporous material with pore sizes less than 2 nm. The isotherms at 800, 1000, 1100, and 1200 °C contain a hysteresis and, therefore, are of type IV in the same classification scheme. Type IV isotherms are associated with the presence of mesopores. The hysteresis associated with type IV isotherms correlates to the formation of the (101) peak in XRD, the formation of layered nanostructures in HRTEM, and the onset of G-band and D-band peak narrowing in Raman spectroscopy. In the CDCs chlorinated at 1100 and 1200 °C, the hysteresis widens presumably as a result of increased mesopore formation. This hypothesis is confirmed by the DFT pore size distribution, Figure 5b. Chlorination at 400 °C resulted in very uniform pores; the fwhm of the pore size distribution for these CDCs (0.6 nm) is smaller than that of single-walled carbon nanotubes. In

(26) Boehm, H. P. *Carbon* **1997**, *35*, 581.
(27) Gogotsi, Y.; Welz, S.; Ersoy, D. A.; McNallan, M. J. *Nature* **2001**, *411*, 283.
(28) Weltz, S. Identification of carbon structures synthesized by chlorination of SiC and TiC. Ph.D. Dissertation, University of Illinois at Chicago, 2003.
(29) Kusunoki, M.; Rokkaku, M.; Suzuki, T. *Appl. Phys. Lett.* **1997**, *71*, 2620.
(30) Zheng, J.; Eckström, T. C.; Gordeev, S. K.; Jacob, M. *J. Mater. Chem.* **2000**, *10*, 1039.
(31) Ekström, T.; Jacob, M.; Zheng, J.; Berius-Henning, P.; Palmqvist, U.; Leis, J.; Perkson, A. Method for Producing a Nanotubular Carbon Material and the Material Produced Thereby. PCT, 2001; WO 01/16023 A1.
(32) Perkson, A.; Leis, J.; Arulepp, M.; et al. *Carbon* **2003**, *41*, 1729.
(33) Leis, J.; Perkson, A.; Arulepp, M.; Kaarik, M.; Svensson, G. *Carbon* **2001**, *39*, 2043.
(34) Gregg, S. J.; Sing, K. S. W. *Adsorption, Surface Area and Porosity*; Academic Press: London, 1967.

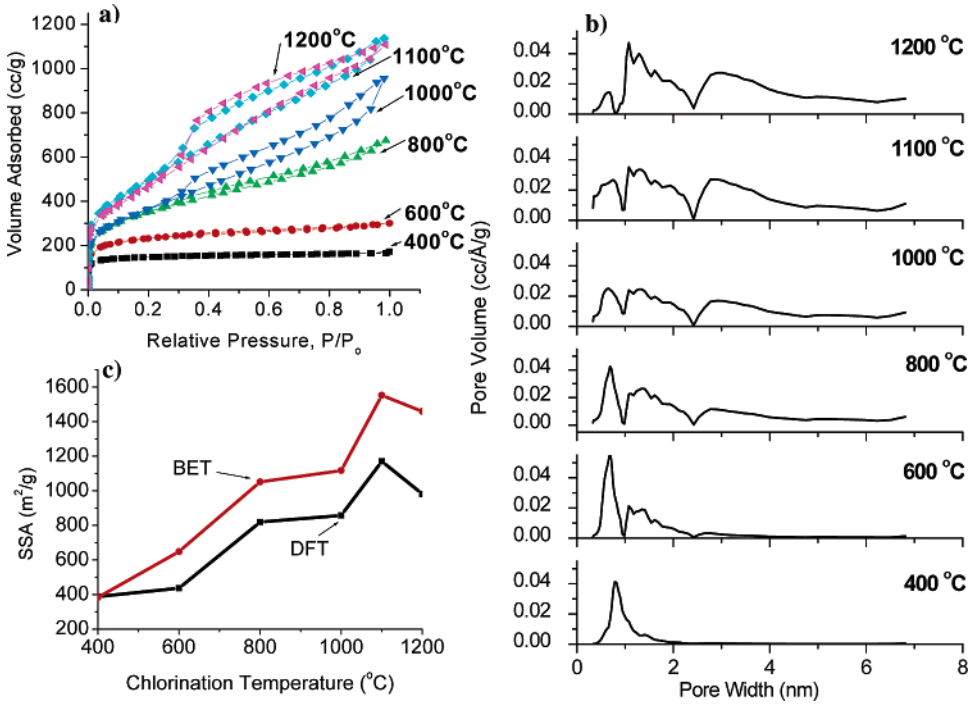

Figure 5. Argon sorption analysis of CDC. (a) Argon adsorption isotherms for chlorination temperatures of 600, 800, 1000, 1100, and 1200 °C. Isotherms at 400 and 600 °C are of type I, the rest are of type IV. (b) DFT pore size distribution at varying chlorination temperatures. (c) BET and DFT specific surface area.

powder produced at 600 °C and below, the majority of the pores are under 2 nm. Higher chlorination temperatures resulted in an increased amount of mesopores, viz. pores widths greater than 2 nm. As the chlorination temperature increases to 1200 °C, the pore size distribution broadens with significant micro- and mesopores.

The observed changes in the pore structure are inherently connected to changes in the microstructure of the CDCs. It is fair to assume that uniform, relatively small pores formed during chlorination at lower temperatures are associated with the amorphous structures (Figure 4a), while the less uniform, and larger pores formed at higher synthesis temperatures are linked to the graphitic ribbon network structure (Figure 4c,d). Mesopore formation can be attributed to pores forming between graphitic ribbons, while imperfections in graphitic ribbons as well as lingering amorphous regions tend toward micropore formation.

The CDC graphitization trends observed herein, increasing chlorination temperature resulting in increasing graphitization, are similar to those observed in Ti_3SiC_2,[12] TiC,[35] and Al_4C_3.[33] Also similar to CDCs produced from Ti_3SiC_2[11,12] and Al_4C_3,[33] the CDCs obtained in this work occasionally formed nanotube-like structures at the intermediate chlorination temperature of 800 °C. However, no significant effect on sorption properties was observed with the formation of these nanostructures. Due to the presence of both micro- and mesopores at 800 °C and above, a broad pore size distribution obtained here is unlike the CDC obtained from Ti_3SiC_2, which contained primarily micropores at similar temperatures.[11,12] In addition to CDC produced from Ti_2AlC, type IV isotherms have also been observed in CDC derived from Al_4C_3 at a chlorination temperature as low as 500 °C,[33] and from TiC at a chlorination temperature of 1000 °C in the presence of a catalyst.[35] Apart from the effect of graphitization, the formation of mesopores in Ti_2AlC as compared to Ti_3SiC_2, also a layered ternary carbide, may stem from the carbon atom separation within the original carbide unit cell. Ti_2AlC's unit cell contains 2 carbon atoms over a 1.36 nm distance in the *c*-direction, while Ti_3SiC_2's unit cell contains 4 carbon atoms over a 1.7671 nm distance in the *c*-direction. The difference in *a*-direction length is marginal between the two structures.

BET and DFT theories were used to determine the SSAs, henceforth referred to as S_{BET} and S_{DFT}, respectively. Both S_{BET} and S_{DFT} (Figure 5c) increased with increasing chlorination temperatures, reaching a maximum of 1552 m^2/g at ~1100 °C, and then appeared to decrease at higher temperatures. The difference in absolute values between S_{BET} and S_{DFT} (Figure 5c) was expected as both types of calculations are based on different assumptions, which might not be justified with the utmost accuracy for all of the materials under study. The BET theory assumes the initial formation of an Ar monolayer, followed by the development of multilayers as the pores are filled. Also, while it is well established that this model gives adequate SSA values for mesoporous materials, it may not be as accurate when micropores (<1−2 nm) are present.

The increase in SSA with increasing chlorination temperatures (Figure 5c) is inconsistent with the presence of smaller pores at the lower chlorination temperatures because smaller pores are expected to yield higher SSA for the same theoretical total pore volume. According to energy dispersive spectroscopy (EDS) analyses (data not shown), samples prepared at low temperatures had a stronger Cl signal than

(35) Leis, J.; Perkson, A.; Arulepp, M.; Nigu, P.; Svensson, G. *Carbon* **2002**, *40*, 1559.

those made at the higher temperatures, up to 11 at. %. This observation suggests that the pores of these samples were filled with trapped chlorine and/or chlorides, resulting in low effective SSAs. It is also possible that some of the pores were too small to be fully accessible to the Ar molecules. The CDC produced at a higher processing temperature showed a smaller Cl signal, as low as 1 at. %, suggesting that the Cl molecules were removed from the pores more efficiently, increasing S_{BET}.

Above 800 °C, graphitic ribbon structures started to form. The fact that the interlayer spacing between graphene layers is close to interplanar spacing in graphite (0.335 nm), which is too small for the Ar atoms to fit between, would explain the reduction in SSA at the higher temperatures.

The trend of increasing SSA with increasing chlorination temperature is similar to that observed in other CDCs, including ones produced from TiC, when no catalyst is present,[35] but is opposite from that found in Al_4C_3 CDCs.[33] The SSA of the CDC produced herein at 1100 °C surpasses that of Al_4C_3-derived carbons produced at all chlorination temperatures[33] and is close to the maximum SSA of CDCs synthesized from TiC (1580 m^2/g) chlorinated at 800 °C.

The CDC produced herein at the higher temperatures may be useful for applications requiring high surface area and relatively large pores, such as electrodes in supercapacitors[36] or adsorbents of organic molecules. Furthermore, Ti_2AlC-derived carbons produced at low chlorination temperatures may possess even higher SSAs than reported herein. Further work is needed and is being carried out, to attempt to remove the residual chlorides that are presumably clogging the micropores, and thus provide an increase in the SSA and the pore volume.

(36) Chmiola, J.; Yushin, G.; Dash, R. K.; Hoffman, E. N.; Fischer, J. E.; Barsoum, M. W.; Gogotsi, Y. *Electrochem. Solid−State Lett.* **2005**, in press.

Summary

Nanoporous carbon was produced from Ti_2AlC powders via chlorination in the temperature range 400−1200 °C. The graphitic nature of the CDC structure increased with chlorination temperature. At chlorination temperatures of 800 °C, sharply curved graphitic ribbons reminiscent of multiwalled nanotubes were observed. At processing temperatures of 1000−1200 °C, the graphitic ribbons widened forming a network. Chlorination temperatures below 600 °C produced CDC having type I sorption isotherms, corresponding to microporous carbon. Higher chlorination temperatures resulted in mesoporous carbon, having a broad pore size distribution and type IV isotherms.

Acknowledgment. We are grateful to Dr. T. El-Raghy of 3-ONE-2, Vorhees, NJ, for providing samples and for many fruitful discussions. Support for this work was provided by Arkema, NSF grant DMR-235173, and NSF IGERT Fellowship. The purchase of the Raman spectrometer and environmental SEM was supported by NSF grants DMR-0115546 and BES-0216343. HRTEM and X-ray diffraction were performed in LRSM, University of Pennsylvania.

CM047739I